Interlayer breathing and shear modes in few-layer black phosphorus

2016 J. Phys.: Condens. Matter 28 165401

(http://iopscience.iop.org/0953-8984/28/16/165401)

IOP Publishing

Journal of Physics: Condensed Matter

J. Phys.: Condens. Matter **28** (2016) 165401 (10pp)

doi:10.1088/0953-8984/28/16/165401

Interlayer breathing and shear modes in few-layer black phosphorus

Jin-Wu Jiang[1], **Bing-Shen Wang**[2] **and Harold S Park**[3]

[1] Shanghai Institute of Applied Mathematics and Mechanics, Shanghai Key Laboratory of Mechanics in Energy Engineering, Shanghai University, Shanghai 200072, People's Republic of China
[2] State Key Laboratory of Semiconductor Superlattice and Microstructure and Institute of Semiconductor, Chinese Academy of Sciences, Beijing 100083, People's Republic of China
[3] Department of Mechanical Engineering, Boston University, Boston, MA 02215, USA

E-mail: jwjiang5918@hotmail.com

Received 8 December 2015, revised 25 February 2016
Accepted for publication 26 February 2016
Published 18 March 2016

Abstract

The interlayer breathing and shear modes in few-layer black phosphorus are investigated for their symmetry and lattice dynamical properties. The symmetry groups for the even-layer and odd-layer few-layer black phosphorus are utilized to determine the irreducible representation and the infrared and Raman activity for the interlayer modes. The valence force field model is applied to calculate the eigenvectors and frequencies for the interlayer breathing and shear modes, which are explained using the atomic chain model. The anisotropic puckered configuration for black phosphorus leads to a highly anisotropic frequency for the two interlayer shear modes. More specifically, the frequency for the shear mode in the direction perpendicular to the pucker is less than half of the shear mode in the direction parallel with the pucker. We also report a set of specular interlayer modes having the same frequency for all few-layer black phosphorus with layer numbers *N* being a multiple of 3, because these modes manifest themselves as collective vibrations of atoms in specific layers. The optical activity of the collective modes enables possible experimental identification for these modes.

Keywords: breathing mode, shear mode, few-layer black phosphorus, group symmetry

(Some figures may appear in colour only in the online journal)

1. Introduction

Heterostructures are a sequential stacking of two different two-dimensional (2D) layered materials [1], which are coupled together via interlayer van der Waals interactions. Characterization of the interlayer coupling in the heterostructures can be done using a lattice dynamical analysis. Specifically, the interlayer breathing (B) mode and shear (C) mode directly represent the interlayer coupling properties in the layered materials. The frequency for the *B* mode is depending on the number of layers, so this mode can be used to determine the number of layers of the heterostructure, while the *C* mode gives insight into the friction between two neighboring 2D layers.

The *C* mode in few-layer graphene was examined experimentally by Tan *et al* in 2012 [2]. The frequency for the highest-frequency *C* mode depends on the layer number (N) as $\sqrt{1+\cos(\pi/N)}$, which was explained by the chain model, and is around 30 cm^{-1} in few-layer graphene. Due to its low frequency, the *C* mode can be excited easily, so it is sensitive to the near-Dirac point quasi-particles [2]. In particular, the *C* mode is easily excited during cross-plane thermal transport in the layered materials, due to its low frequency. The scattering between the *C* mode and the acoustic modes may play an important role for the cross-plane thermal transport in the layered materials. More recently, two experiments found that the signal of the *C* mode can be enhanced by folding the graphene layers [3, 4]. The *B* mode in few-layer graphene has also been studied by several groups [5, 6].

As another important 2D layered material, few-layer MoS_2 has also attracted significant attention for its interlayer modes. Several experiments have measured the N dependence for the frequency of the interlayer B mode and C mode in few-layer MoS_2 [7–10]. The frequency of the interlayer B mode decreases with increasing layer number, while the C mode exhibits the opposite behavior.

Few-layer black phosphorus (FLBP) is another emerging 2D layered material with that shows an N-dependent band gap [11, 12]. However, few works have been performed for the phonon modes in black phosphorus. The phonon dispersion for bulk black phosphorus was measured [13, 14] in 1980s. The experiment was explained by Kaneta *et al* using the valence force field model (VFFM) [15, 16] or the adiabatic bond charge model [17]. While the layer number dependence for symmetry analysis of the interlayer B mode and C mode in the FLBP was studied by Ribeiro-Soares *et al* [18], there have not been any studies on the layer number dependence for the frequency of the interlayer B and C modes in FLBP, in which an important and interesting effect to quantity is that of the intrinsically puckered BP geometry on the interlayer modes. We thus analyze the lattice dynamics properties for the interlayer B mode and C mode in the FLBP.

In this paper, we study the symmetry and the lattice dynamical properties for the interlayer B mode and C mode in FLBP. The symmetry groups for the FLBP with even or odd layer numbers are compared. Using these symmetry groups, we analyze the symmetry for the interlayer B and C modes, including their irreducible representations and their infrared (IR) and Raman activity. The VFFM is utilized to compute the eigenvectors and frequencies for the interlayer B and C modes, while the calculated results are explained by the linear chain model. As a result of the intrinsic geometric anisotropy in the puckered configuration of BP, the two interlayer C modes have very different frequencies. Furthermore, we present a set of collective interlayer modes in FLBP with layer number $N = 3i$ with integer i. The frequencies for these collective modes are independent of the layer number and these modes are optically active, so they should be experimentally measurable.

2. Symmetry analysis for BP structure

2.1. Bulk BP

There are eight atoms in the orthorhombic cell for bulk BP. The bases for the orthorhombic cell are as follows,

$$\vec{A}_1 = a\hat{e}_x, \tag{1}$$

$$\vec{A}_2 = b\hat{e}_y, \tag{2}$$

$$\vec{A}_3 = c\hat{e}_z, \tag{3}$$

where $\hat{e}_x$, $\hat{e}_y$, and $\hat{e}_z$ are unit vectors in the three cartesian directions. The lattice constants $a = 4.1766$ Å and $b = 3.2197$ Å are computed from the Stillinger–Weber potential [19]. The VFFM used for the interlayer interaction is linear, so it cannot be used to optimize the interlayer structure. We thus take the value of the lattice constant $c = 10.587$ Å from [12].

The primitive unit cell for the bulk BP contains four atoms [20]. The bases for the primitive unit cell are,

$$\vec{a}_1 = \vec{A}_1, \tag{4}$$

$$\vec{a}_2 = \frac{1}{2}(\vec{A}_2 - \vec{A}_3), \tag{5}$$

$$\vec{a}_3 = \frac{1}{2}(\vec{A}_2 + \vec{A}_3). \tag{6}$$

Each unit cell can be labelled by a lattice vector $\vec{R}_{l_1l_2l_3} = l_1\vec{a}_1 + l_2\vec{a}_2 + l_3\vec{a}_3$, with l_1, l_2, and l_3 as three integers. The lattice vector corresponds to a translation symmetry operation, $\hat{T}_{l_1l_2l_3}$, which translates the bulk BP by a lattice vector $\vec{R}_{l_1l_2l_3}$.

The point group for the bulk BP is $D_{2h} = \{E, C_{2z}, C_{2y}, C_{2x}, i, \sigma_{xy}, \sigma_{yz}, \sigma_{zx}\}$. C_{2z} is the rotation for π around the z-axis, i is the inversion symmetry and σ_{xy} is the reflection with respect to the $z = 0$ plane. Four of these eight symmetry operations, C_{2z}, C_{2x}, σ_{xy}, and σ_{yz}, are accompanied by the following nonprimitive translations,

$$\vec{\tau}_B = \frac{1}{2}(\vec{A}_1 + \vec{A}_3). \tag{7}$$

The translational symmetry and the point group together construct the space group (D_{2h}^{18}) of bulk BP; i.e. $D_{2h}^{18} = \hat{T}_{l_1l_2l_3} \otimes D_{2h}$.

The reciprocal vectors are determined by the bases for the primitive unit cell through the relation

$$\vec{b}_i \cdot \vec{a}_j = 2\pi\delta_{ij}, \tag{8}$$

which gives,

$$\vec{b}_1 = \frac{2\pi}{a}\hat{e}_x, \tag{9}$$

$$\vec{b}_2 = \frac{2\pi}{b}\hat{e}_y - \frac{2\pi}{c}\hat{e}_z, \tag{10}$$

$$\vec{b}_3 = \frac{2\pi}{b}\hat{e}_y + \frac{2\pi}{c}\hat{e}_z. \tag{11}$$

$\vec{b}_1$ is in x-direction, while $\vec{b}_2$ and $\vec{b}_3$ lie in the yz plane. The first Brillouin zone for bulk BP is shown in figure 1.

The Z point in the first Brillouin zone plays an important role in the present work. The wave vector for the B mode and C mode in the bulk BP is located at the Z point of the first Brillouin zone, and not at the Γ point of the first Brillouin zone. This can be demonstrated as follows. The wave vector for the Z point is,

$$\vec{k}_Z = \frac{1}{2}(-\vec{b}_2 + \vec{b}_3). \tag{12}$$

We shall treat the unit cell containing the four atoms (1, 2, 3, 4) in figure 2 as the (0, 0, 0) unit cell. The lattice vector for this unit cell is $\vec{R}_{000} = 0$. This unit cell (0, 0, 0) is in the same plane as the unit cell containing atoms (5, 6, 7, 8). The lattice vector for the latter unit cell is $\vec{R}_{011} = \vec{A}_2 = \vec{a}_2 + \vec{a}_3$, so its phase factor in the Bloch theory is $\vec{k}_Z \cdot \vec{R}_{011} = 0$, which means that the phase factors for the unit cells in the same BP plane are the same. The lattice vector for the unit cell

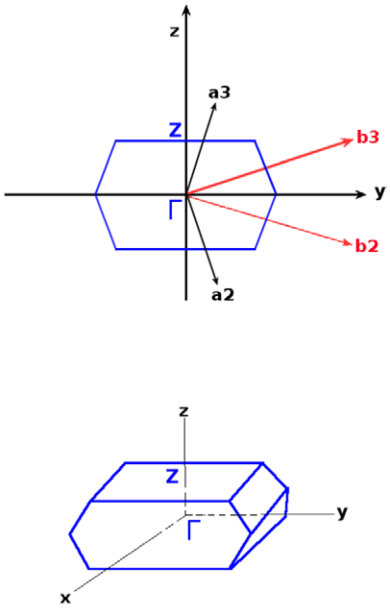

Figure 1. The first Brillouin zone for bulk BP. Top is the projection of the first Brillouin zone onto the yz plane. Bottom is the three-dimensional first Brillouin zone for bulk BP.

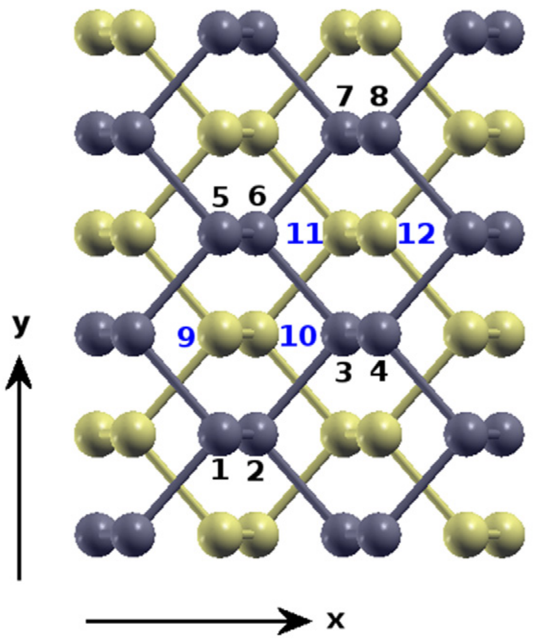

Figure 2. Top view of bulk BP. The two BP layers are displayed by different colors. The x-direction is perpendicular to the pucker, and the y-direction is parallel with the pucker.

containing atoms (9, 10, 11, 12) is $\vec{R}_{010} = \vec{a}_2$, with the phase factor as $\vec{k}_Z \cdot \vec{R}_{010} = -\pi$. This unit cell (0, 1, 0) is in a different layer from the (0, 0, 0) unit cell. It shows that the vibration for the two BP layers in bulk BP are out-of-phase at the Z point. We therefore have demonstrated that the phonon modes at the Z point correspond to the relative vibrations between the two BP layers in bulk BP. The B mode and C mode studied in the present work describe the relative breathing or shearing motion of the two BP layers, so the wave vectors for these modes are located at the Z point.

Table 1. The irreducible representation for the D_{2h} group at the Z point in the Brillouin zone.

	E	C_{2z}	C_{2y}	C_{2x}	i	σ_{xy}	σ_{xz}	σ_{yz}
$A_g = Z_2^+$	1	1	1	1	1	1	1	1
$B_{1g} = Z_3^+$	1	1	-1	-1	1	1	-1	-1
$B_{2g} = Z_1^+$	1	-1	1	-1	1	-1	1	-1
$B_{3g} = Z_4^+$	1	-1	-1	1	1	-1	-1	1
$A_u = Z_2^-$	1	1	1	1	-1	-1	-1	-1
$B_{1u} = Z_3^-$	1	1	-1	-1	-1	-1	1	1
$B_{2u} = Z_1^-$	1	-1	1	-1	-1	1	-1	1
$B_{3u} = Z_4^-$	1	-1	-1	1	-1	1	1	-1

Note: The two symbols for the irreducible representation are listed in the first column.

There are twelve phonon modes at the Γ point or Z point for bulk BP, corresponding to the four atoms in the primitive unit cell. The symmetry for these phonon modes can be analyzed according to the point group (D_{2h}) of bulk BP. Table 1 lists the eight irreducible representations for the point group D_{2h}. There are two symbols for each irreducible representation in the first column of table 1. The first symbol is for phonon modes at the Γ point, while the second symbol is for the phonon modes at the Z point in the first Brillouin zone.

Table 2 shows the symmetry analysis for phonon modes at the Γ point or the Z point in the first Brillouin zone. $\Gamma^{\rm vib} = \Gamma^{\rm a.s.} \otimes \Gamma^{\rm vec}$ is the vibrational representation, with $\Gamma^{\rm a.s.}$ as the permutation representation and $\Gamma^{\rm vec}$ as the vector representation. The decomposition of the vibrational representation gives the irreducible representation for each phonon mode at the Z point in the first Brillouin zone. The vibrational representation can be decomposed as follows, using the character table method,

$$\Gamma^{\rm vib} = 2Z_2^+ \oplus Z_3^+ \oplus 2Z_1^+ \oplus Z_4^+ \oplus Z_2^- \oplus 2Z_3^- \oplus Z_1^- \oplus 2Z_4^-. \quad (13)$$

The twelve phonon modes at the Z point in the first Brillouin zone belong to these 12 irreducible representations on the right-hand side of equation (13). From the eigenvector, it can be determined that the B mode in bulk BP belongs to the Z_4^- irreducible representation, the C_x mode belongs to the Z_3^- irreducible representation, and the C_y mode belongs to the Z_2^- irreducible representation. These results are shown in the second line of table 3.

The IR activity for each phonon mode can be analyzed by decomposing the vector representation in the following,

$$\Gamma^{\rm vec} = Z_1^- \oplus Z_3^- \oplus Z_4^-. \quad (14)$$

The vector representation is three-dimensional, so there are three one-dimensional irreducible representations in the resulting decomposition. This result predicts that phonon modes corresponding to these three irreducible representations will be IR-active in the optical scattering process. According to this result, the B mode (Z_4^-) and C_x mode (Z_3^-) in bulk BP are IR-active, while the C_y mode (Z_2^-) is IR inactive.

The Raman activity for each phonon mode can be determined by decomposing the six-dimensional tensor

Table 2. Symmetry analysis for phonon modes in bulk BP (Γ point and Z point) and FLBP (Γ point).

	Point group	Mode number	$\Gamma^{\rm vib}$	Γ^{IR}	Γ^{R}
Bulk at Γ point	D_{2h}	12	$2A_g \oplus B_{1g} \oplus 2B_{2g} \oplus B_{3g} \oplus A_u \oplus 2B_{1u} \oplus B_{2u} \oplus 2B_{3u}$	$B_{1u} \oplus B_{2u} \oplus B_{3u}$	$3A_g \oplus B_{1g} \oplus B_{2g} \oplus B_{3g}$
Bulk at Z point	D_{2h}	12	$2Z_2^+ \oplus Z_3^+ \oplus 2Z_1^+ \oplus Z_4^+ \oplus Z_2^- \oplus 2Z_3^- \oplus Z_1^- \oplus 2Z_4^-$	$Z_1^- \oplus Z_3^- \oplus Z_4^-$	$3Z_2^+ \oplus Z_3^+ \oplus Z_1^+ \oplus Z_4^+$
FLBP, even N	D_{2h}	$12N$	$2NA_g \oplus NB_{1g} \oplus 2NB_{2g} \oplus NB_{3g} \oplus NA_u \oplus 2NB_{1u} \oplus NB_{2u} \oplus 2NB_{3u}$	$B_{1u} \oplus B_{2u} \oplus B_{3u}$	$3A_g \oplus B_{1g} \oplus B_{2g} \oplus B_{3g}$
FLBP, odd N	D_{2h}	$12N$	$2NA_g \oplus NB_{1g} \oplus 2NB_{2g} \oplus NB_{3g} \oplus NA_u \oplus 2NB_{1u} \oplus NB_{2u} \oplus 2NB_{3u}$	$B_{1u} \oplus B_{2u} \oplus B_{3u}$	$3A_g \oplus B_{1g} \oplus B_{2g} \oplus B_{3g}$

Note: The total number of phonons is listed in the third column. Phonon modes are classified by the irreducible representations of $\Gamma^{\rm vib}$ in the fourth column. The irreducible representations of the IR and Raman-active modes are listed in the fifth and sixth columns, respectively. N is the layer number.

Table 3. The irreducible representation for the B mode and C modes.

	B_1 mode	C_{x1} mode	C_{y1} mode	B_2 mode	C_{x2} mode	C_{y2} mode
Bulk	Z_4^- (IR)	Z_3^- (IR)	Z_2^- (No)	/	/	/
FLBP, even N	A_g (R)	B_{2g} (R)	B_{3g} (R)	B_{1u} (IR)	B_{3u} (IR)	B_{2u} (IR)
FLBP, odd N	A_g (R)	B_{3u} (IR)	B_{2u} (IR)	B_{1u} (IR)	B_{2g} (R)	B_{3g} (R)
Layer dependence	$\sqrt{1-\cos\frac{\pi}{N}}$	$\sqrt{1+\cos\frac{\pi}{N}}$	$\sqrt{1+\cos\frac{\pi}{N}}$	$\sqrt{1-\cos\frac{2\pi}{N}}$	$\sqrt{1+\cos\frac{2\pi}{N}}$	$\sqrt{1+\cos\frac{2\pi}{N}}$

Note: IR or Raman-activity is listed in the parentheses, where 'No' indicates optically inactive. N is the layer number.

Table 4. VFFM parameters.

	α_1	α_2	α_3
Reference [16]	0.321	−0.01	0.015
Present work	0.281	−0.067	0.03

Note: The original parameters from [16] are listed in the second line. The third line lists optimized parameters used in the present work. All parameters are in the unit of eV Å^{-2}. The corresponding potential is $V=\frac{1}{2}\alpha[(\vec{u}_i-\vec{u}_j)\cdot\hat{e}_{ij}]^2$, where $\vec{u}_j$ is the displacement for atom j and $\hat{e}_{ij}$ is the unit vector from atom i to atom j.

Table 5. Frequency (in cm^{-1}) for the B mode, C_x mode, and C_y mode in bulk BP.

	B	C_x	C_y
Exp	87.1	19.4	51.6
Reference [16]	92.8 (↑ 6.5%)	21.1 (↑ 8.8%)	53.5 (↑ 3.7%)
Present work	87.1 (0%)	20.0 (↑ 3.1%)	51.7 (↑ 0.2%)

Note: Theoretical results from [16] (3rd line) and the present work (4th line) are compared with experiments (2nd line). The values in parentheses (3rd line and 4th line) are the relative difference between the theoretical prediction and the experiment.

representation, $\Gamma^{v\times v}$. The bases for the tensor representation are x^2+y^2, z^2, x^2-y^2, xy, xz, and yz. The tensor representation is decomposed as follows,

$$\Gamma^{v\times v}=3Z_2^+\oplus Z_3^+\oplus Z_1^+\oplus Z_4^+.$$

According to this decomposition result, none of the three interlayer modes is Raman active in bulk BP.

The above decomposition results for phonon modes at the Z point in bulk BP are shown in the third line of table 2. The symmetry analysis for phonon modes at the Γ point in the first Brillouin zone of bulk BP are shown in the second line of table 2. The symmetry for the three interlayer modes for bulk BP are shown in the second line of table 3.

2.2. Few-layer BP

The FLBP studied in the present work has the same stacking order as the bulk BP as shown in figure 2, which can be regarded as the AB stacking, while the group symmetry for the AA stacking FLBP was analyzed in a previous work [18]. There is no translational symmetry in the z-direction for FLBP. Hence, the orthorhombic cell for the FLBP is the primitive unit cell in this structure. The bases are $\vec{A}_1$ and $\vec{A}_2$. There are $4N$ atoms in the primitive unit cell of the FLBP. These eight point group symmetry operations in the bulk BP are still symmetry operations in the FLBP, but accompanied by different nonprimitive translations.

For even-layer FLBP, the point group for the FLBP with even N is D_{2h}. Two of these eight symmetry operations, C_{2z} and σ_{yz}, are accompanied by the following nonprimitive translations,

$$\vec{\tau}_{E1}=\frac{1}{2}(\vec{A}_1+\vec{A}_2). \tag{15}$$

Another two symmetry operations, C_{2x} and σ_{xy}, are accompanied by the following nonprimitive translations,

$$\vec{\tau}_{E2}=\frac{1}{2}\vec{A}_1. \tag{16}$$

The irreducible representation for each phonon mode at the Γ point is found by decomposing the vibrational representation for the FLBP with even N. The symmetry analysis results are shown in the fourth line of table 2.

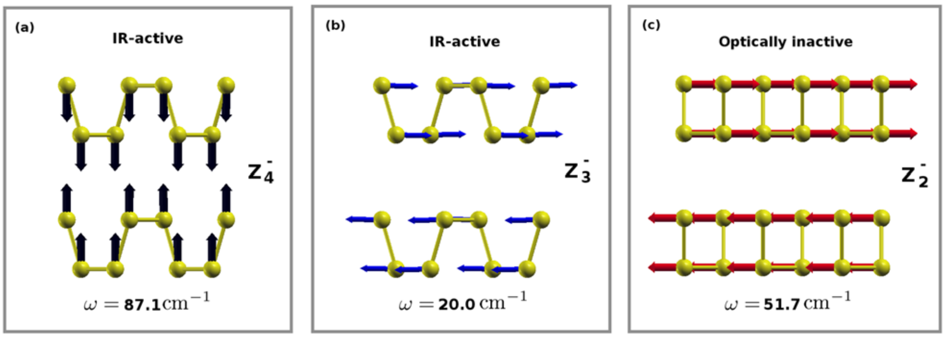

Figure 3. Eigenvectors for the three interlayer modes in bulk BP. (a) B mode. (b) C_x mode. (c) C_y mode. The arrow on top of each atom represents the vibrational amplitude of the eigenvector.

For the B mode, we are interested in the first lowest-frequency B (B_1) mode and the second lowest-frequency B (B_2) mode in FLBP. The eigenvectors for these two B modes are shown in figure 4. For the C mode, we are interested in the first highest-frequency C mode (C_{x1} or C_{y1}) and the second highest-frequency C (C_{x2} or C_{y2}) mode. The eigenvectors for these C modes are shown in figures 5 and 6. The third line of table 3 shows the symmetry for these modes in the FLBP with even N.

For odd-layer FLBP, the point group is also D_{2h}. Four of these eight symmetry operations, C_{2z}, C_{2x}, σ_{xy}, and σ_{yz}, are accompanied by the following nonprimitive translations,

$$\vec{\tau}_O = \frac{1}{2}(\vec{A}_1 + \vec{A}_2). \tag{17}$$

The symmetry analysis for phonon modes at Γ point in the odd-layer FLBP are shown in the fifth line of table 2. The symmetry for the interlayer modes are shown in the fourth line of table 3. The IR-activity and Raman-activity are also shown in the table.

3. Interaction potential

The intralayer interaction is described by a recently developed Stillinger–Weber potential [19]. We apply the VFFM for the interlayer coupling between two adjacent BP layers [16]. This VFFM contains the following bond stretching interaction,

$$V = \frac{1}{2}\alpha[(\vec{u}_i - \vec{u}_j)\cdot\hat{e}_{ij}]^2\,, \tag{18}$$

where $\vec{u}_j$ is the displacement for atom j, $\hat{e}_{ij}$ is the unit vector from atom i to atom j, $\alpha = \alpha_1$, α_2, and α_3 are the parameters for the first-, second-, and third-nearest-neighbor interlayer interactions, respectively. Figure 2 shows the configuration for bulk BP. The interlayer first-nearest-neighbor distance is the distance between atoms 9 and 2, i.e. $d_1 = 3.7311$ Å. The interlayer second-nearest-neighbor distance is the distance between atoms 9 and 3, i.e. $d_2 = 3.8520$ Å. The interlayer third-nearest-neighbor distance is the distance between atoms 9 and 7, i.e. $d_3 = 4.9612$ Å.

The original VFFM parameters from [16] are listed in the second column in table 4. These parameters are further optimized in the present work by fitting the frequencies of interlayer phonon modes in bulk phosphorus, and are also listed in table 4. After optimization, frequencies for the interlayer B mode and C mode in bulk BP agree well with the experimental results as shown in table 5.

The phonon modes are calculated using GULP [21]. Table 5 lists the frequency for the B mode and two C modes in bulk BP. Due to the intrinsic geometric anisotropy due to the puckered configuration, the frequency for the interlayer shear mode in the x-direction (C_x) is quite different from the frequency of the interlayer shear mode in the y-direction (C_y). The frequencies of the interlayer modes from the optimized VFFM parameters agree quite well with the experiment, with a maximum error of about 3% for the C_x mode. The eigenvectors for the interlayer modes in the bulk BP are shown in figure 3. The figure is produced using XCRYSDEN [22].

Table 4 shows that α_2 is negative in both the original VFFM parameter set and the optimized parameter set. A negative VFFM parameter implies that BP becomes unstable under high pressure. This pressure induced structure instability was investigated experimentally by Yamada *et al* [14].

4. Numerical results

For the interlayer mode in the layered structure, each layer can be regarded as a single atom. The entire layered structure can thus be considered as a single atomic chain with free boundary conditions at the two ends. This atomic chain model has been successfully applied to simulate the interlayer modes in few-layer graphene [2] and few-layer MoS_2 [9]. It can be assumed that each atom in the chain only interacts with its nearest-neighboring atoms. The eigenvector for the phonon mode τ in the chain model is

$$u_j^\tau \propto \cos\left[\frac{(\tau-1)(2j-1)\pi}{2N}\right], \tag{19}$$

where τ is the mode index, N is the total atom number and j is the site index for each atom. The first mode ($\tau = 1$) is the acoustic mode. The frequency for mode τ is

$$\omega_\tau = \sqrt{\frac{\beta}{2\mu\pi^2c^2}\left\{1-\cos\left[\frac{(\tau-1)\pi}{N}\right]\right\}}. \tag{20}$$

$\mu = 1.53\times10^{-26}$ kgÅ^{-2} is the mass per unit area of the single-layer BP, c is the speed of light in cm s^{-1} and β is the force constant per unit area.

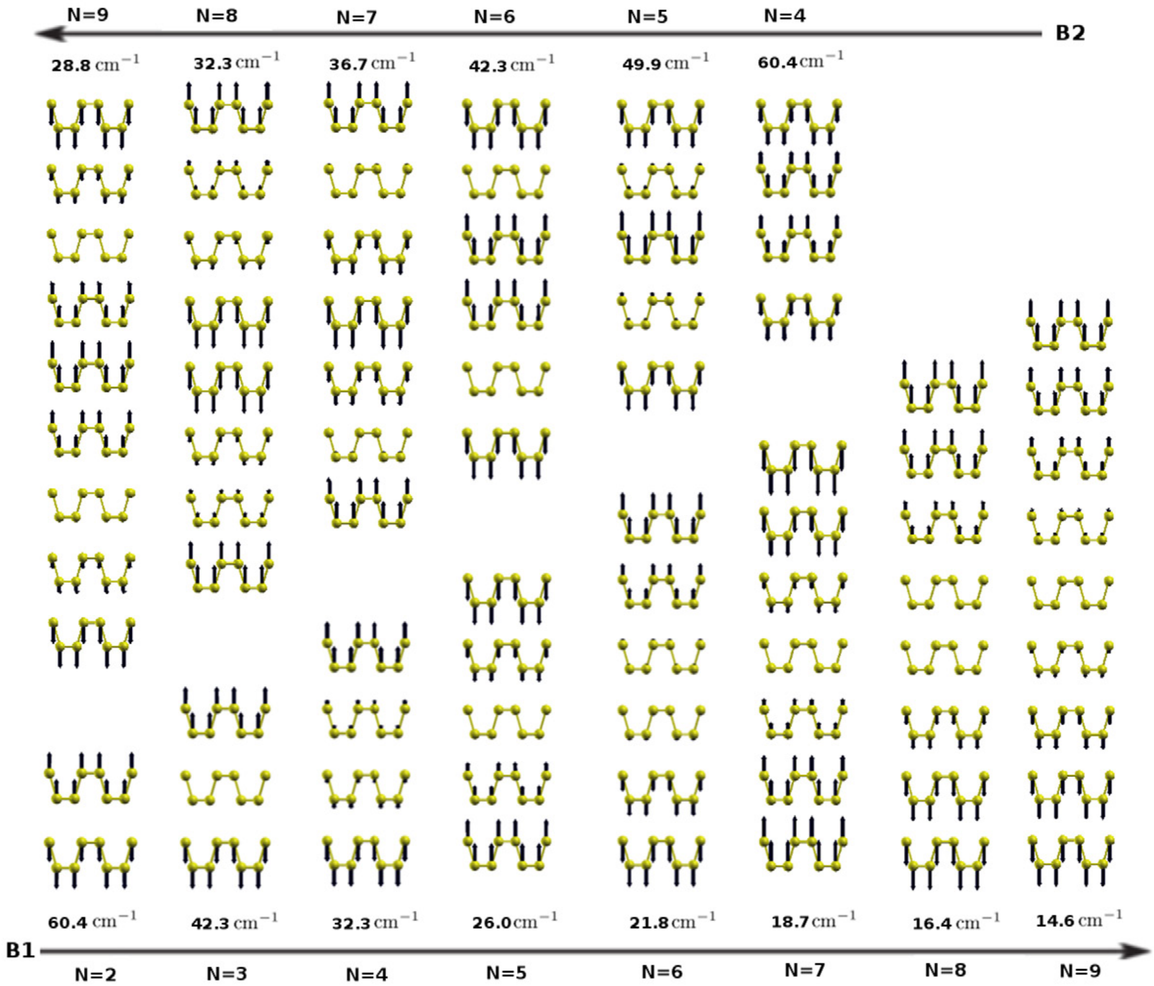

Figure 4. Eigenvectors and frequencies for two B modes. Bottom is the lowest-frequency B mode. Top is the second-lowest-frequency B mode.

We discuss four sets of interlayer phonon modes for FLBP in this section. The eigenvectors for these modes are shown in figures 4–8. The layer number dependence for the frequency are shown in figures 9 and 10.

The first set is the two B modes, i.e. B_1 mode and B_2 mode. The B_1 mode corresponds to the phonon mode with $\tau = 2$ in the chain model. Figure 4 shows that the eigenvector of the B_1 mode indeed follows the prediction of the chain model, i.e. $u_j^2 \propto \cos\left[\frac{(2j-1)\pi}{2N}\right]$. The N-dependence for the frequency of the B_1 mode is shown in figure 9, where the black solid line illustrates a perfect fitting of the frequency for the B_1 mode to the function $\omega_2 = \sqrt{\frac{\beta_B}{2\mu\pi^2c^2}\left[1-\cos\left(\frac{\pi}{N}\right)\right]}$. These results show that the B_1 mode can be well described by the chain model. From the fitting of the frequency, we get the breathing force constant parameter $\beta_B = 9.8 \times 10^{19}$ Nm^{-3} for the chain model.

The B_2 mode corresponds to $\tau = 3$ in the chain model. Its eigenvector is shown in figure 4, which agrees with the prediction of the chain model, i.e. $u_j^3 \propto \cos\left[\frac{(2j-1)\pi}{N}\right]$. The N-dependence for the frequency of B_2 mode is shown in figure 10, where the black solid line shows that the frequency for the B_2 mode can be well fitted to the function $\omega_3 = \sqrt{\frac{\beta_B}{2\mu\pi^2c^2}\left[1-\cos\left(\frac{2\pi}{N}\right)\right]}$. The fitting parameter $\beta_B = 9.8 \times 10^{19}$ Nm^{-3} is exactly the same as that obtained from the B_1 mode. This agreement further confirms the success of the chain model in the description of the layered structure.

The second set of phonon modes are the interlayer C_x modes in FLBP, including the first highest-frequency C_{x1} mode and the second highest-frequency C_{x2} mode. This mode can also be described by the chain model. The C_{x1} mode corresponds to the phonon mode with $\tau = N$ in the chain model. The eigenvector of the C_{x1} mode is shown in figure 5. This eigenvector follows the function $u_j^N \propto \cos\left[\frac{(N-1)(2j-1)\pi}{2N}\right]$. The N-dependence for the frequency of the C_{x1} mode is shown in figure 9, which is fitted to the function $\omega_N = \sqrt{\frac{\beta_{Cx}}{2\mu\pi^2c^2}\left[1+\cos\left(\frac{\pi}{N}\right)\right]}$. The fitting parameter $\beta_{Cx} = 5.5 \times 10^{18}$ Nm^{-3} is the force constant for the transverse motion in the x-direction for the chain model.

The C_{x2} mode corresponds to $\tau = N - 1$ mode in the chain model. Its eigenvector is shown in figure 5, which coincides with the eigenvector of the chain model with $\tau = N - 1$ in equation (19). The frequency for the C_{x2} is shown in figure 10.

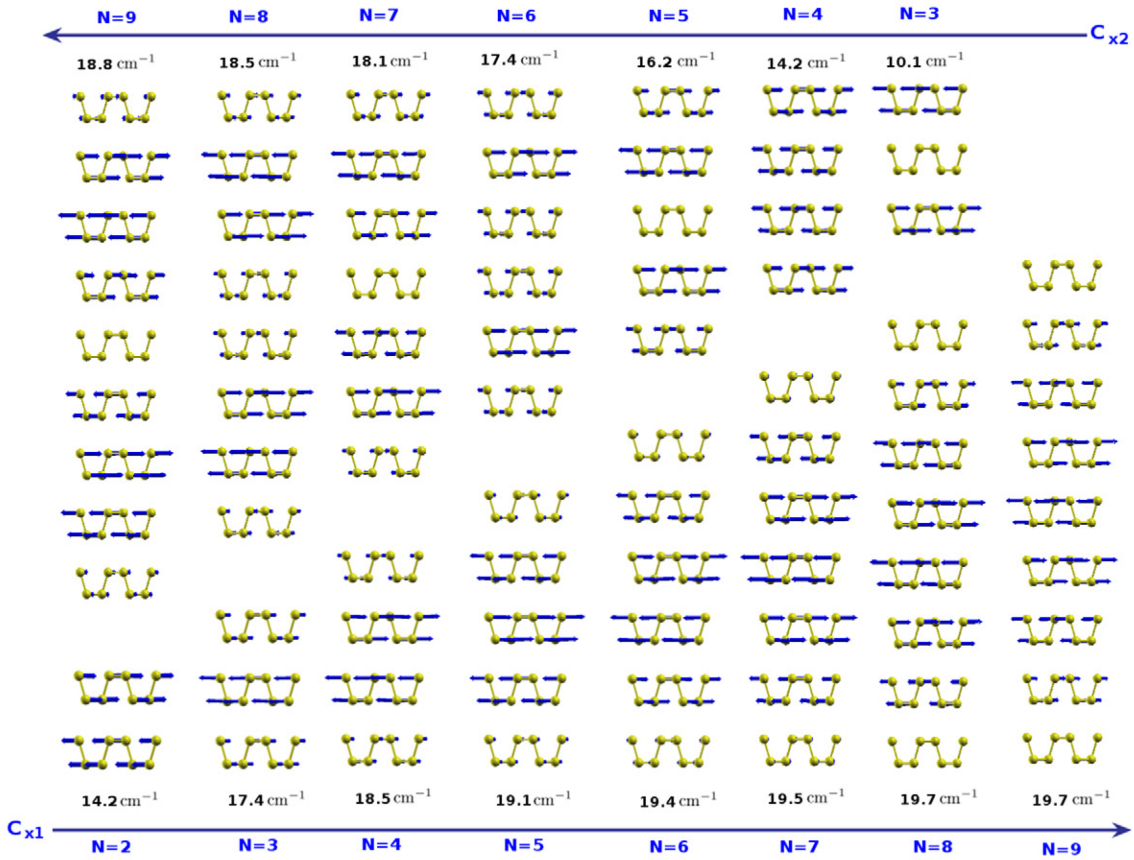

Figure 5. Eigenvectors and frequencies for two C_x modes. Bottom is the highest-frequency C_x mode. Top is the second-highest-frequency C_x mode.

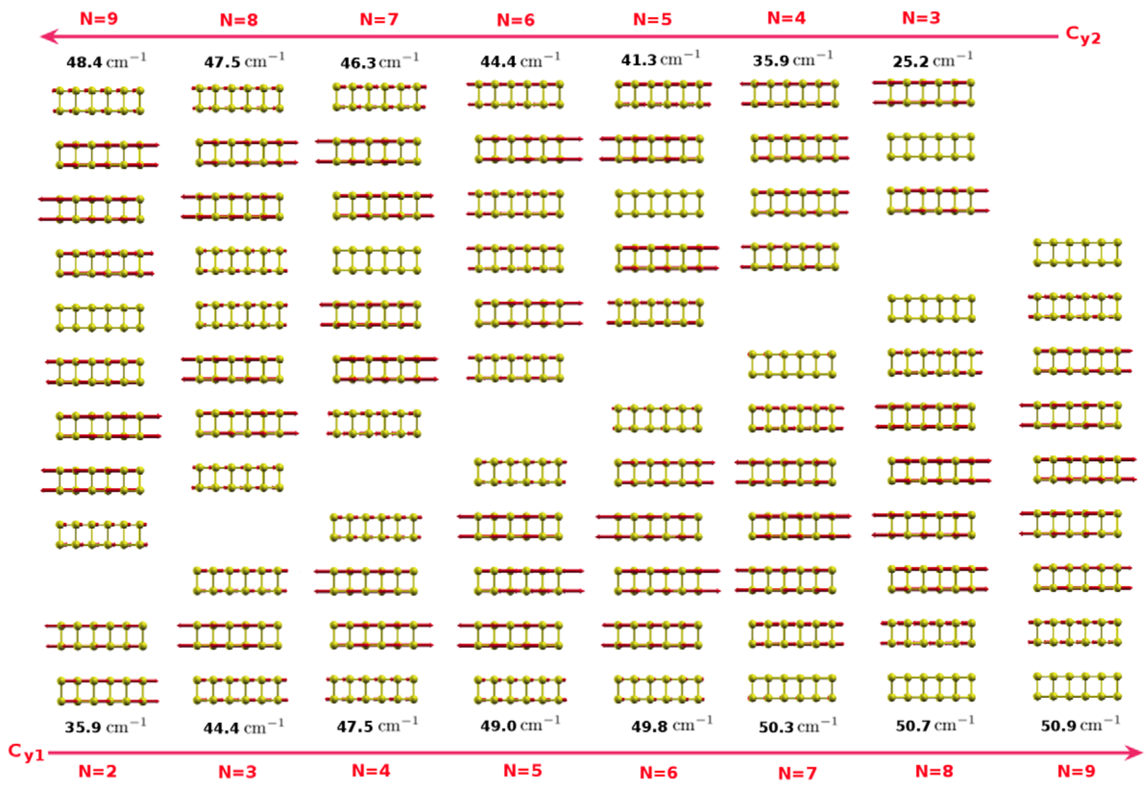

Figure 6. Eigenvectors and frequencies for two C_y modes. Bottom is the highest-frequency C_{y1} mode. Top is the second-highest-frequency C_{y2} mode.

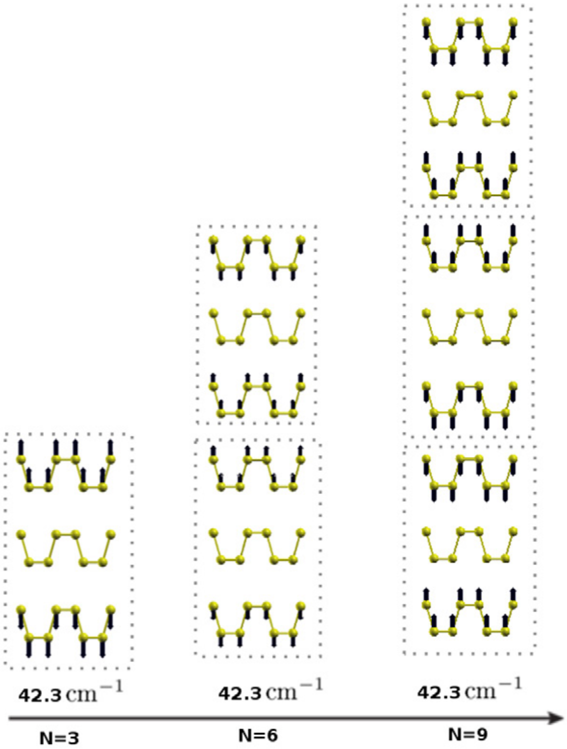

Figure 7. Interlayer collective B modes with the same frequency for FLBP with $N = 3$, 6, and 9 (from left to right). The eigenvector can be regarded as the collective vibration of the small segments (dotted rectangles).

The N-dependence of the frequency is also consistent with the chain model prediction by equation (20) with $\tau = N - 1$.

The third set of phonon modes are two interlayer C_y modes in FLBP; i.e. the first highest frequency C_{y1} mode and the second highest-frequency C_{y2} mode. These modes can also be described by the chain model. C_{y1} mode corresponds to the phonon mode with $\tau = N$ in the chain model, while the C_{y2} mode corresponds to the phonon mode with $\tau = N - 1$ in the chain model. The eigenvectors of these two modes are shown in figure 6. They agree with the chain model prediction in equation (19). The frequencies of these two modes are shown in figures 9 and 10. They can be fitted by the frequency in the chain model in equation (20). The fitted parameter $\beta_{Cy} = 3.6 \times 10^{19}$ Nm^{-3} is the force constant for the y-directional transverse motion for the chain model. The transverse force constant is about 1.28×10^{19} Nm^{-3} for the few-layer graphene [2] and 2.7×10^{19} Nm^{-3} in the few-layer MoS_2 [9]. These values are sandwiched between the two transverse force constants β_{Cx} and β_{Cy} in FLBP.

The fourth set of phonon modes are the collective vibration modes corresponding to the mode index $\tau = \frac{N}{3} + 1$ in the chain model. According to equation (19), the eigenvector for this set of vibration modes is $u_j \propto \cos(\frac{2j-1}{6}\pi)$. Hence, we have $u_j = 0$ for $j = 2, 5, 8, ..., 3i + 2$ with integer i; $u_j \propto \cos(\pi/6)$ for $j = 1, 4, 7, ..., 3i + 1$; $u_j \propto -\cos(\pi/6)$ for $j = 3, 6, 9, ..., 3i$. The frequency for this set of vibration modes is independent of layer number N, i.e. $\omega_\tau = \sqrt{\frac{\beta}{4\mu\pi^2c^2}}$. For instance, figure 7 shows the collective B mode in FLBP with layer number $N = 3i$ ($i = 1, 2, 3, ...,$). The frequencies of these collective B modes are independent of the layer number. For $N = 6$, the third and fourth BP layers have the same vibrational displacement, so the overall displacement can be regarded as a collective vibration of two segments (displayed by dotted rectangles). Furthermore, the displacement for each segment is the same as the displacement for $N = 3$. As a result, the frequency for the phonon mode in 6-layer BP is the same as the frequency for 3-layer BP. Similarly, for $N = 9$, the structure can be deconstructed into three collective segments. Each segment has the same displacement as FLBP with $N = 3$, so the frequency for the phonon mode in FLBP with $N = 9$ is the same as the FLBP with $N = 3$. Figure 8 shows a similar phenomenon for the collective C_x mode and C_y modes in FLBP. As shown in table 3, this set of phonon modes are optically active, so we expect that it will be possible to identify these FLBP phonon modes experimentally. It should be noted that equation (20) is applicable to other layered structures,

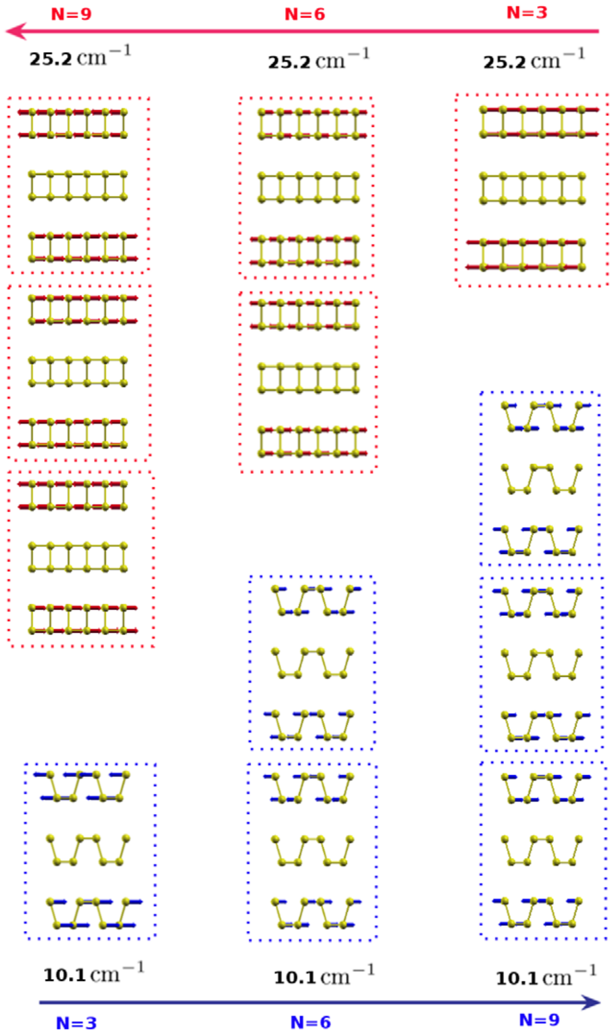

Figure 8. Interlayer collective C modes with the same frequency for FLBP with $N = 3$, 6, and 9. Bottom is the C_x mode, and top is the C_y mode.

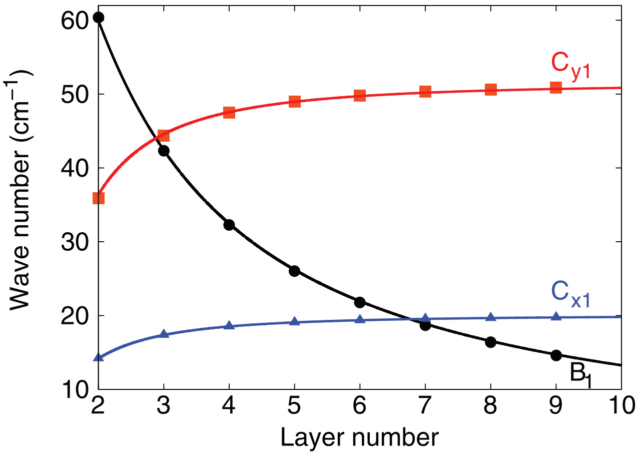

Figure 9. The layer dependence for some interlayer modes. B_1 is the lowest-frequency interlayer B mode. C_{x1} is the highest-frequency interlayer C mode in the x-direction. C_{y1} is the highest-frequency interlayer C mode in the y-direction. Lines are fitting functions according to the chain model.

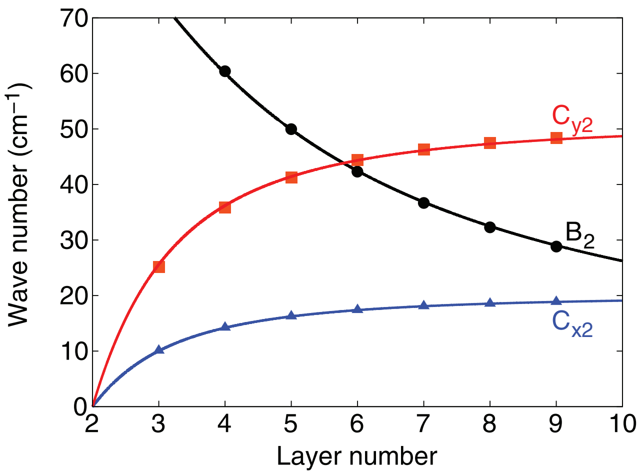

Figure 10. The layer dependence for some interlayer modes. B_2 is the second lowest-frequency interlayer B mode. C_{x2} is the second highest-frequency interlayer C mode in the x-direction. C_{y2} is the second highest-frequency interlayer C mode in the y-direction. Lines are fitting functions according to the chain model.

so this set of collective modes are a general feature for all layered structures, including few-layer graphene, few-layer MoS_2, and few-layer BP.

We note that our manuscript was put publicly on arXiv in December 2014 [23]. During the submission process of the present manuscript, there have been several experiments measuring the frequency of the interlayer B and C modes in the FLBP [24–30]. The frequency of the B_1 mode in bilayer BP is about 62.7 cm^{-1} by Ling *et al* [24], or 67.5 by Dong *et al* [25], which are quite close with 60.4 cm^{-1} in the present work. The frequency of the B_1 mode in four-layer BP is about 35 cm^{-1} by Luo *et al* [26], which is quite close to 32.3 cm^{-1} in the present work. Some theoretical studies also emerge on the layer number dependence of the interlayer B and C modes very recently [31, 32].

5. conclusion

To summarize, we have analyzed the lattice dynamical properties for the interlayer B and C modes in FLBP. The symmetry group for the FLBP with even layer numbers is compared with the FLBP with odd layer numbers. The symmetry properties for the interlayer modes are determined based on the symmetry groups. The IR and Raman activity for the phonon modes is also determined. We applied the VFFM to compute the eigenvectors and frequencies for the interlayer modes, which can be successfully explained by the chain model. The two C modes have very different frequencies, due to the anisotropic puckered configuration for the BP layer. We found a particular set of collective phonon modes with the same frequency in the FLBP with layer number $N = 3i$ (i integer). These collective phonon modes have a constant frequency with respect to the layer number.

Acknowledgments

The work is supported by the Recruitment Program of Global Youth Experts of China, the National Natural Science Foundation of China (NSFC) under Grant No. 11504225, and the start-up funding from Shanghai University. HSP acknowledges the support of the Mechanical Engineering department at Boston University.

References

[1] Neto A H C and Novoselov K 2011 *Rep. Prog. Phys.* **74** 082501
[2] Tan P H *et al* 2012 *Nat. Mater.* **11** 294300
[3] Tan P-H, Wu J-B, Han W-P, Zhao W-J and Zhang X 2014 *Phys. Rev.* B **89** 235404
[4] Cong C and Yu T 2014 *Nat. Commun.* **5** 4709
[5] Jiang J-W, Tang H, Wang B-S and Su Z-B 2008 *Phys. Rev.* B **77** 235421
[6] Lui C H, Malard L M, Kim S, Lantz G, Laverge F E, Saito R and Heinz T F 2012 *Nano Lett.* **12** 55395544
[7] Plechinger G, Heydrich S, Eroms J, Weiss D, Schuller C and Korn T 2012 *Appl. Phys. Lett.* **101** 101906
[8] Zeng H, Zhu B, Liu K, Fan J, Cui X and Zhang Q M 2012 *Phys. Rev.* B **86** 241301
[9] Zhao Y *et al* 2013 *Nano Lett.* **13** 1007
[10] Zhang X, Han W P, Wu J B, Milana S, Lu Y, Li Q Q, Ferrari A C and Tan P H 2013 *Phys. Rev.* B **87** 115413
[11] Liu H, Neal A T, Zhu Z, Tomnek D and Ye P D 2014 *ACS Nano* **8** 4033
[12] Du Y, Ouyang C, Shi S and Lei M 2010 *J. Appl. Phys.* **107** 093718
[13] Fujii Y, Akahama Y, Endo S, Narita S and Shirane Y Y G 1982 *Solid State Commun.* **44** 579
[14] Yamada Y, Fujii Y, Akahama Y, Endo S, Narita S, Axe J D and McWhan D B 1984 *Phys. Rev.* B **30** 2410
[15] Kaneta C, Katayama-Yoshida H and Morita A 1982 *Solid State Commun.* **44** 613
[16] Kaneta C, Katayama-Yoshida H and Morita A 1986 *J. Phys. Soc. Japan* **55** 1213
[17] Kaneta C and Morita A 1986 *J. Phys. Soc. Japan* **55** 1224
[18] Ribeiro-Soares J, Almeida R M, Cancado L G, Dresselhaus M S and Jorio A 2015 *Phys. Rev.* B **91** 205421

[19] Jiang J-W, Rabczuk T and Park H S 2015 *Nanoscale* **7** 6059
[20] Slater J C, Koster G F and Wood J H 1962 *Phys. Rev.* **126** 1307
[21] Gale J D 1997 *J. Chem. Soc. Faraday Trans.* **93** 629
[22] Kokalj A 2003 *Comput. Mater. Sci.* **28** 155
[23] Jiang J-W, Wang B-S and Park H S 2014 Preprint at http://arxiv.org/abs/1412.7587
[24] Ling X, Liang L, Huang S, Puretzky A A, Geohegan D B, Sumpter B G, Kong J, Meunier V and Dresselhaus M S 2015 *Nano Lett.* **15** 4080
[25] Dong S, Zhang A, Liu K, Ji J, Ye Y G, Luo X G, Chen X H, Ma X, Jie Y and Zhang Q 2015 Preprint at http://arxiv.org/abs/1503.06577
[26] Luo X, Lu X, Koon G K W, Neto A H C, Ozyilmaz B, Xiong Q and Quek S Y 2015 *Nano Lett.* **15** 3931
[27] Su L and Zhang Y 2015 *Appl. Phys. Lett.* **107** 071905
[28] Late D J 2015 *ACS Appl. Mater. Interfaces* **7** 5857
[29] Luo Z, Maassen J, Deng Y, Du Y, Garrelts R P, Lundstrom M S, Ye P D and Xu X 2015 *Nat. Commun.* **6** 8572
[30] Wang Y, Cong C, Fei R, Yang W, Chen Y, Cao B, Yang L and Yu T 2015 *Nano Res.* **8** 3944
[31] Hu Z-X, Kong X, Qiao J, Normand B and Ji W 2016 *Nanoscale* **8** 2740
[32] Luo X, Lu X, Cong C, Yu T, Xiong Q and Quek S Y 2015 *Sci. Rep.* **5** 14565